High Sea-Floor Stress Induced by Extreme Hurricane Waves

Hemantha W. Wijesekera, David W. Wang, William J. Teague, and Ewa Jarosz

Naval Research Laboratory, Bldg 1009, Code 7330,
Stennis Space Center, MS 39529

Abstract

Strong surface waves and currents generated by major hurricanes can produce extreme forces at the seabed that scour the seafloor and cause massive underwater mudslides. Our understanding of these forces is poor due to lack of concurrent measurements of waves and currents under these storms. Using unique observations collected during the passage of a category-4 hurricane, Ivan, bottom stress due to currents and waves over the outer continental shelf in the Gulf of Mexico was examined. During the passage of Ivan, the bottom stress was highly correlated with the wind with a maximum of about 40% of the wind stress. The bottom stress was dominated by the wave-induced stresses, and exceeded critical levels at depths as large as 90 m. Surprisingly, the bottom damaging stress persisted after the passage of Ivan for about a week, and was modulated by near-inertial waves.

1. Introduction

Hurricanes can produce extreme forces at the ocean bottom, even on the outer continental shelf. Bottom stresses resulting from near bottom flows are less noticeable than surface winds and waves. These episodic wind events modify and control the near-bottom environment through resuspension and transport of sediments, and redistribution of organisms and chemicals. In the presence of strong surface waves, the combined current-wave stress is considerably larger than the bottom stress associated only with mean currents [e.g., *Grant et al.,* 1984; *Madsen et al.*, 1993; *Cacchione and Drake*, 1982]. Stresses generated by the surface waves over the sea floor of the continental shelf have been often underestimated since wave heights under hurricanes were believed to exceed 20 m or so only in the 100-year storm events. Recently, an extreme wave with a crest-to-trough height of 28 m was measured under Hurricane Ivan and was not considered a rogue wave height but rather a common wave height that can occur under a major hurricane [*Wang et al.,* 2005]. Significant wave heights likely surpassed 21 m and maximum individual wave heights may have exceeded 40 m near the eyewall [*Wang et al.,* 2005].

The Gulf of Mexico (GOM) region provides nearly 30% of the United States oil supply and 20% of its natural gas. Hurricanes are major threats to the integrity of offshore operations over the GOM outer continental shelf. Significant damage can occur to underwater pipelines and to other underwater infrastructures such as oil and gas platforms [*Cruz and Krausmann*, 2008]. There are reportedly at least 50,000 km of pipeline on the seafloor of the GOM [MMS, 2006]. Damage to pipelines, which often is difficult to detect unless the damage is catastrophic, can be more costly to repair than damage to the

43 superstructures on platforms. Major oil leaks from damaged pipelines could have
44 irreversible impacts to the ocean environment. Improved understanding and accurate
45 prediction of hurricane-induced bottom stresses on the seafloor area along hurricane
46 paths can enable better engineering designs to reduce pipeline failures. However,
47 understanding of hurricane-induced extreme bottom stresses is hampered by the lack of
48 direct measurements of near-bottom flow generated by winds and waves under intense
49 storms. Deployments of large numbers of instruments along hurricane tracks are not
50 practically feasible. There are only a few reported wave and current measurements
51 directly under the paths of historical hurricanes. For example, elevated bottom stress and
52 sediment resuspension over the Mid-Atlantic-Bight shelf off the east coast of US were
53 found during the passage of Hurricane Edouard in 1996 [*Dickey et al*., 1998; *Chang et*
54 *al.*, 2001]. The eye of the hurricane passed within 110 km of the mooring site when the
55 maximum wind speed and wave height were about 20 m s^{-1} and 9 m, respectively, and the
56 resuspension of sediments was up to 30 m above the seabed. The maximum bottom stress
57 based on a current-wave interaction model [*Christoffersen and Jonsson*, 1985] was about
58 0.35 N m^{-2}.

59 Measurements of bottom pressures and full water-column current profiles were
60 fortuitously made under the eye of Hurricane Ivan in 2004 by the Naval Research
61 Laboratory (NRL) as part of the Slope to Shelf Energetics and Exchange Dynamics
62 (SEED) project [*Teague et al*., 2007]. Six current-profiler moorings along with wave-tide
63 gauges were deployed on the continental shelf at water depths ranging between 60 and 90
64 m near 29.4^{o}N, 88^{o}W (Figure 1). Ivan passed over the SEED mooring array on
65 September 16 around 0000 UTC as a category-4 storm before making landfall near Gulf

66 Shores, Alabama [*Teague et al*., 2007; *Powell et al.*, 1998]. The measurements indicated
67 that significant wave heights exceeded 20 m; near-bottom wave-induced oscillatory
68 currents were over 2 m s^{-1} [*Wang et al.*, 2005]; and bottom scours exceeded 0.3 m at the
69 60 m isobath [*Teague et al.*, 2007]. Extreme waves, currents, and scours as observed
70 during Ivan are likely produced by other hurricanes.

71 The main objective of this paper is to quantify bottom stress over the continental
72 shelf during the passage of Ivan. The seabed frictional coefficients and bottom stresses
73 were evaluated from the observed near-bottom currents and wave-orbital velocities in
74 combination with the wave-current boundary layer model [e.g., *Christoffersen and*
75 *Jonsson*, 1985]. This study focuses on the growing and relaxation stages of the hurricane.
76 During the growing stage of Ivan (between September 10 and 17, 2004), the coastal
77 ocean was directly forced by accelerating winds from 10 to 50 m s^{-1}, and during the
78 relaxation stage (between September 18 and 25, 2004), surface winds became weak but
79 the circulation was dominated by wind-generated near-inertial currents [*Mitchell et al*.,
80 2005]. The correlation of the bottom stress with the surface wind stress is also
81 investigated.

82

83 **2. Methods**

84 A number of models have been formulated to evaluate wave-induced bottom stress
85 [e.g., *Grant and Madsen*, 1979; *Trowbridge and Madsen*, 1984; *Christoffersen and*
86 *Jonsson*, 1985; *Glenn and Grant*, 1987]. Some advanced models [*Trowbridge and*
87 *Madsen*, 1984; *Glenn and Grant*, 1987] address complex seabed sediment conditions
88 such as armoring and moveable beds. In the following we used a simple fixed flat-bed

89 model described in *Christoffersen and Jonsson* [1985] (hereinafter CJ85), mainly because
90 the exact nature of the seabed sediment conditions were not known during the passage of
91 Ivan. CJ85 is similar to the most commonly-used model [*Grant and Madsen*, 1979], but
92 utilizes an iterative approach for computing frictional coefficients based on bottom
93 currents, wave statistics, and sediment grain sizes. CJ85 was used to evaluate bottom
94 stress and sediment resuspension over the Mid-Atlantic-Bight shelf off the east coast of
95 United States in the wake of Hurricane Edouard and Hortense in 1996 [*Dickey et al*.,
96 1998; *Chang et al.*, 2001]. The selection of a particular model would not make a
97 significant difference in the general conclusions presented here. However, the estimated
98 bottom stress during the storm should be treated as a lower bound, since the bottom could
99 be a movable bed, which tends to generate a higher-roughness scale than what was used
100 in the fixed-bed representation of the critical bottom stress [e.g., *Madsen et al*., 1993].
101 Comparison of several wave-current boundary-layer models are given in [*Soulsby et al*.,
102 1993].

103 The iterative procedure described in CJ85 computes the wave friction factor (f_W),
104 the current friction factor (f_C), and then the combined current-wave stress (τ_{CW}) on the
105 sea bed, where $\tau_{CW} = 0.5 f_W \rho u_W^2 m$; ρ is the density of sea water; m describes the relation
106 between the current and the wave, and is a function of f_W , f_C , wave orbital velocity (u_W),
107 current velocity (u_C), and angle between the current and the wave; f_C depends on the
108 Nikuradse roughness (k_N) [*Nikuradse*, 1933], the apparent roughness (k_A), and the height
109 of the current boundary layer (h). The bottom stress due to the mean current
110 is: $\tau_C = 0.5 f_C \rho u_C^2$. The combined current-wave-dissipation rate (ε_{CW}) and the current-
111 dissipation rate (ε_C) were estimated using the following relationships:

$\varepsilon_{CW} = (\tau_{CW} / \rho)^{3/2} / (\kappa\, z)$ and $\varepsilon_C = (\tau_C / \rho)^{3/2} / (\kappa\, z)$, where z is the height from the bottom, and κ is the von Karman constant (0.4).

The near-bottom flow field was composed of a background mesoscale component driven by a basin-scale wind stress curl in addition to low-frequency currents ranging from inertial to sub-inertial flows [*Teague et al.*, 2007]. The most-significant bottom currents were directly wind driven with superimposed high-frequency oscillatory currents driven by surface waves and swells. Bottom stresses and dissipation rates were computed from background currents and wave-orbital velocities at the seafloor. The bottom wave-orbital velocities were estimated from 512-s burst-sampling records of wave-induced dynamic pressure measurements at 0.25 m above the bottom [*Wang et al.*, 2005] based on linear wave theory. Ocean currents at 0.25 m above the bottom were approximated by extrapolating near-bottom velocities from acoustic Doppler current profilers (ADCPs) while assuming the constant stress layer with a logarithmic velocity profile (i.e., "law of the wall") extends from the seabed to the depth of the first measured velocity above the ADCP. Typically the thickness of the wall boundary layer is about 10% of the thickness of the bottom mixed layer. During the passage of Hurricane Ivan, the current structure was found to be frictionally driven with overlapping surface and bottom boundary layers [*Mitchell et al.*, 2005] suggesting that the entire water column over the shelf was either weakly stratified or well mixed. Therefore, a 6- to 9-m-thick wall boundary layer is expected near the vicinity of the sea floor. The moorings rested on a sandy seabed with grain sizes varying from 0.06 mm to 1 mm with a median size of about 0.3 mm [*Sawyer et al.*, 2001]; therefore k_N was approximated to be about 0.3 mm. The alignment angles between the currents and wave orbital velocities were not known, and therefore, the

currents and waves were assumed to be in the same direction and the alignment angle was set to zero for the computations. Since wave statistics were only sampled every 8 hours, estimates of τ_{CW} and ε_{CW} were limited to 3 times per day. The bottom currents from the ADCP were sampled at 15-minute intervals, and therefore τ_C and ε_C were computed at a higher sampling rate by interpolating 8-h estimates of f_C into the ADCP sampling rate. By following *Madsen et al.* [1993], the wave-orbital velocity was approximated as the root-mean-square amplitude of a sinusoidal wave, where $u_w = \sqrt{2}\sigma_u$, and σ_u is the standard deviation of orbital-velocity fluctuations based on the 512-s burst-sampling record of pressure at 0.25 m above the bottom [*Wang et al.*, 2005]. The surface wind field over mooring locations was constructed by combining NDBC buoy winds with Ivan post storm wind analysis products [*Wang et al.*, 2005; *Powell et al*., 1998].

3. Observations

A dramatic increase in bottom stress and dissipation rate was found at all six mooring locations during the passage of Ivan. At the 60-m isobath, the current-wave stress (τ_{CW}) was enhanced by two orders of magnitude (Figure 2c) and the current-wave dissipation rate (ε_{CW}) was enhanced two to three orders of magnitude (Figure 2d) as the wind speed accelerated from 10 m s^{-1} to 50 m s^{-1}, during which wave-orbital bottom velocity intensified from O(mm s^{-1}) to O(1 m s^{-1}) (Figure 2a, b). At the 90-m isobath, wave-orbital velocities were relatively weak, background currents were strong (Figure 2g), and the current-wave stress was a factor of two smaller than that at the 60-m isobath (Figure 2c,h). Peak bottom stresses at moorings M1 to M6 were 0.47, 0.58, 0.84, 0.62, 0.48, and 0.34 N m^{-2}, respectively. Some of the differences in current-wave stresses at

158 different mooring locations were related to the undersampling of wave-orbital velocities
159 at an 8-h interval and depth dependence of wave statistics. Out of the six moorings, M3,
160 which was located to the right of Ivan's path (Figure 1), had the strongest bottom stress,
161 largest wave-orbital velocity (Figure 2b,c) and the largest surface-wave height of about
162 28 m [*Wang et al.*, 2005]. There was an increase in background stress levels following
163 the hurricane; the current stress (τ_C), averaged over the mooring array, prior to Ivan was
164 $7\text{x}10^{-3}$ N m^{-2} [$1\text{x}10^{-6}$, $4\text{x}10^{-2}$] while that stress after Ivan was $30\text{x}10^{-3}$ N m^{-2} [$20\text{x}10^{-6}$,
165 $27\text{x}10^{-2}$], where minimum and maximum stresses are given in the brackets.
166 The ADCP echo intensity (Figure 2e,j) reflects the concentration of particles in the
167 water column [*Deines*, 1999]. Therefore the timing and the duration of the resuspension
168 of sediments (during which $\tau_{CW} >$ the critical stress) can be identified from the echo
169 intensity. The observed critical stress is consistent with the spiking of echo intensity. The
170 resuspension occurred as the wind speed exceeded ~ 15 m s^{-1} and lasted for two days
171 over both 60-m and 90-m isobaths. After the passage of Ivan, the resuspension continued
172 at the 60-m isobath, and was modulated by near-inertial waves (Figure 2e), but it was
173 considerably weaker at the 90-m isobath (Figure 2j). The intensity of the ADCP echo was
174 enhanced up to 25 m above the instrument, implying that sediments were resuspended to
175 about 25 m above the seabed (Figure 2e,j).
176 The relationship between bottom stress (τ_{CW}, τ_C) and wind speed (U_{10}) during the
177 growing stage of the hurricane was studied by averaging bottom stresses into appropriate
178 bins as a function of the wind speed (Figure 3). The impact of surface waves on the
179 bottom stress was not important for winds less than 8 m s^{-1}. There was a rapid build up
180 in τ_{CW} as U_{10} increased from 10 m s^{-1} to 15 m s^{-1}. The growth of τ_{CW} slowed down for $U_{10} >$

181 20 m s^{-1}, and τ_{CW} was approximately proportional to U_{10}^2. τ_C was also proportional to U_{10}^2
182 for most of the wind record. On average τ_C was a factor of 4 smaller than τ_{CW} based on
183 the wave-orbital velocity, $u_w = \sqrt{2}\sigma_u$ (Figure 3). The current-wave stress can be
184 approximated as $\tau_{CW} \approx 4\times10^{-4}U_{10}^2$ for winds higher than 15 m s^{-1}, which in turn implies
185 that $\tau_{CW} \approx C\tau_S$, where τ_S is the surface wind stress, and the proportionality constant,
186 $C = 4\times10^{-4}/\rho_{air}C_D^S$; ρ_{air} is the density of air, and C_D^S is the surface drag coefficient. For
187 $C_D^S = (1.5-2.5)\times10^{-3}$ (13), C is ~ 0.15 - 0.2. Sensitivity of τ_{CW} to the strength of the orbital
188 velocity was examined by choosing the wave-orbital velocity as significant wave-orbital
189 velocity (u_{ws}), where, $u_{ws} = 2\sigma_u$, and the wave-orbital velocity as maximum wave-orbital
190 velocity (u_{WM}). It is clear from Figure 3 that τ_{CW} is highly sensitive to the magnitude of
191 the wave-orbital velocity chosen. The estimate of τ_{CW} for the maximum wave-orbital
192 velocity, u_{WM} is about a factor of 2 larger than that for the root-mean-square
193 velocity, $\sqrt{2}\sigma_u$.
194
195 **4. Summary and Discussion**
196 During the passage of Ivan, the bottom stress, energy dissipation rate, and
197 resuspension of sediment were controlled primarily by dissipative processes induced by
198 surface waves, whereas during the relaxation stage of Ivan, wave-orbital velocities
199 became small and the bottom stress, dissipation rates, and resuspension of sediments
200 were determined by the observed bottom current. The strongest stresses occurred to the
201 right of the storm path. Bottom stresses exceeded critical levels on the outer continental
202 shelf at depths as large as 90 m. Bottom damaging stresses occurred during the passage of

the storm and for about a week after storm passage. The bottom stress associated with the ocean currents peaked at wind speeds of about 30 m s^{-1} and then may actually have decreased as the wind speed increased, paralleling the surface drag reduction at high winds [*Jarosz et al*., 2007; *Powell et al*., 2003]. The current-wave induced bottom stress continued to increase as the wind speed increased, and was about 15%-20% of the surface wind stress, where $u_w = \sqrt{2}\sigma_u$. The maximum stress based on the maximum wave-orbital velocity was found to be as large as 40% of the surface wind stress. On average, bottom stresses induced by ocean bottom-current interactions with ocean surface-wave-related currents were a factor of 4 larger than the bottom stresses attributed to ocean bottom currents alone.

The occurrence of critical bottom stresses on the outer shelf must be considered in the engineering design of structures on the bottom and in determining where pipe lines should be buried and not just laid on top of the ocean floor. Some climate models have predicted an increase in the frequency of intense hurricanes as the climate warms [*Bender et al*., 2010]. The cumulative effects of enhanced bottom stresses and associated transport of large quantities of sediment along the shelf edge could be a trigger mechanism for a slumping or mass-wasting event at the shelf break.

Acknowledgments. This work was supported by the Office of Naval Research as part of the NRL's basic research project SEED under program element grant 0601153N. Comments given by Jim Richman were greatly appreciated.

References

Bender, M. A., T.R. Knutson, R.E. Tuleya, J.J. Sirutis, G.A. Vecchi, S.T. Garner, and I.M. Held (2010), Modeled impact of anthropogenic warming on the frequency of intense Atlantic hurricanes, *Science, 327*, 454-458.

Cacchione, D. A., and D. A. Drake (1982), Measurements of storm generated bottom stress on the continental shelf, *J. Geophys. Res., 87*, 1952-1961.

Chang, G. C., T. D.. Dickey, and A. J. Williams III (2001), Sediment resuspension over a continental shelf during Hurricane Edouard and Hortense, *J. Geophys. Res.,106*, 9517 -9531.

Christoffersen, J. B., and I. G. Jonsson (1985), Bed friction and dissipation in a combined current and wave motion, *Ocean Eng.*, 12, 387-423.

Cruz, A. M., and E. Krausmann, (2008), Damage to offshore oil and gas facilities following hurricane Katrina and Rita: An overview, *J. Loss Prevention Process Ind., 21*, 620-626.

Deines, K. L., (1999), Backscatter estimation using broadband acoustic doppler current profilers, IEEE 6th working conference on current measurement, San Diego, 249-253, DOI:10.1109/CCM.1999.755249.

246 Dickey, T. D., G. C. Chang, Y. C. Agrawal, A. J. Williams, III, and P. S. Hill (1998),
247 Sediment resuspension in the wakes of Hurricane Edouard and Hortense, *Geophys. Res.*
248 *Lett.*, *25*, 3533-3536.
249
250 Glen, S. M., and W. D. Grant (1987), A suspended sediment stratification correction for
251 the combined wave and current flows, *J. Geophys. Res.*, *92*, 8244-8264.
252
253 Grant, W. D., A. J. Williams III, and S. M. Glenn (1984), Bottom stress estimates and
254 their predication on the northern California continental shelf during CODE-1: The
255 importance of wave-current interaction, *J. Phys. Oceanogr*., *14*, 506-527.
256
257 Grant, W. D., and O.S. Madsen (1979), Combined wave and current interaction with
258 rough bottom, *J. Geophys. Res.*, *84*, 1797-1808.
259
260 Jarosz, E., D.A. Mitchell, D.W. Wang, and W.J. Teague (2007), Bottom-up
261 determination of air-sea momentum exchange under a major tropical cyclone, *Science,*
262 *315*, 1707-1709 .
263
264 Madsen, O. S., L. D. Wright, J. D. Boon, and T. A. Chisholm (1993), Wind stress, bed
265 roughness and sediment suspension on the inner shelf during an extreme strom event,
266 *Cont. Shelf Res.*, *13*, 1303-1324.

267 Mitchell, D. A., W.J. Teague, E. Jarosz, and D.W. Wang (2005), Observed currents over
268 the outer continental shelf during Hurricane Ivan, *Geophys. Res. Lett.*, 32,
269 doi:10.1029/2005GL023014.
270
271 Minerals Management Service (MMS) (2006), Pipeline damage assessment from
272 Hurricanes Katrina and Rita. Technical Report No. 448 14183, 104pp.
273
274 Nikuradse, J., Stromungsgesetz in rauhren rohren, vdi-forschungsheft 361 (1933).
275 (English translation: Laws of flow in rough pipes), 1950. Technical report, NACA
276 Technical Memo 1292. National Advisory Commission for Aeronautics, Washinton, DC.
277
278 Powell, M. D., S. H. Houston, L. R. Amat, and N. Morisseau-Leroy (1998), The HRD
279 real-time hurricane wind analysis system, *J. Wind Eng. Ind. Aerodyn., 77&78*, 53-64.
280
281 Powell, M. D., P. J. Vickery, and T. A. Reinhold (2003), Reduced drag coefficient for
282 high wind speeds in tropical cyclones, *Nature*, *422*, 279-283.
283
284 Teague, W. J., E. Jarosz, D.W. Wang, and D.A. Mitchell (2007), Observed oceanic
285 response over the upper continental slope and outer shelf during Hurricane Ivan, *J. Phys.*
286 *Oceanogr*., 37, 2181-2206.
287
288 Trowbridge, J. H., and O. S. Madsen (1984), Turbulent wave boundary layers, 1, Model
289 formulation and first-order solution, *J. Geophys. Res.*, *89*, 7989-7997.

290 Sawyer, W. B., C. Vaughan, D. Lavoie, Y. Furukawa, N. Carnaggio, J. Maclean, and
291 E. Populis (2001), Report No. NRL/MR/7430-01-8548, Naval Research Laboratory,
292 Stennis Space Center, Miss..
293
294 Soulsby, R. L., L. Hamm, G. Klopman, D. Myrhaug, R. R. Simons, and G. P. Thomas
295 (1993), Wave-current interaction within and outside the bottom boundary layer, *Coastal*
296 *Engineering, 21*, 41-69.
297
298 Wang, D. W., D.A. Mitchell, W.J. Teague, E. Jarosz, and M.S. Hulbert (2005), Extreme
299 waves under hurricane Ivan, *Science, 309*, 896-896.
300

301 **Figure Captions**

302 **Figure 1.** Path of Ivan (dashed red line). The crosses denote the center of Ivan for the
303 time marked in red. Mooring locations at 60-m and 90-m isobaths are marked in solid
304 circles (M1-M6). The yellow triangle is the National Data Buoy Center (NDBC) buoy
305 42040. Contours indicate bathymetry in meters. The translation speed of the hurricane
306 was about 6 m s^{-1}.
307

308 **Figure 2**.Observations at M3 (left panels) and M6 (right panels) mooring locations. Time
309 series of (a, f) 10-m wind speed U_{10} in m s^{-1} and radial distance to Ivan's center (black) in
310 kilometers [*Powell et al*., 1998]. (b, g) Root-mean-square estimate of wave-orbital speed,
311 $u_W = \sqrt{2}\sigma_u$ (red dots), where σ_u is the standard deviation of orbital-velocity fluctuations
312 based on the 512-s burst-sampling record of pressure, and ADCP currents u_C (black line)

313 at 0.25 m above the bottom. Units are in m s^{-1}. (c, h) Combined current-wave stress τ_{CW}

314 (red dots) and current stress τ_C (black line) in N m^{-2}. (d, i) Estimated current-wave

315 dissipation rate ε_{CW} (red dots) and current dissipation ε_C (black line) at 0.25 m above the

316 bottom. Units are in W kg^{-1}. (e, j) ADCP echo intensity as function of height (H) in

317 meters from the bottom

318

319 **Figure 3.** Mean stress at 0.25 m above the bottom vs wind speed U_{10} during the growing

320 stage of Ivan. The bottom stress based on mean current (u_c) is the solid black line with

321 diamonds. The combined current-wave stress τ_{CW} based on bottom orbital-velocities:

322 $u_w = \sqrt{2}\sigma_u$, significant wave-orbital velocity $u_{WS} = 2\sigma_u$, and maximum orbital-velocity,

323 u_{WM} are marked in dots (red), squares (blue), and open circles (magenta) , respectively.

324 Error bars are given by the thin red vertical lines and denote maximum and minimum

325 values of τ_{CW} for $u_w = \sqrt{2}\sigma_u$. The dashed black and red lines are not mathematical fits to

326 the data, but represent $\tau = 10^{-4} U_{10}^2$ (black), $\tau = 4 \times 10^{-4} U_{10}^2$ (red).

327

328

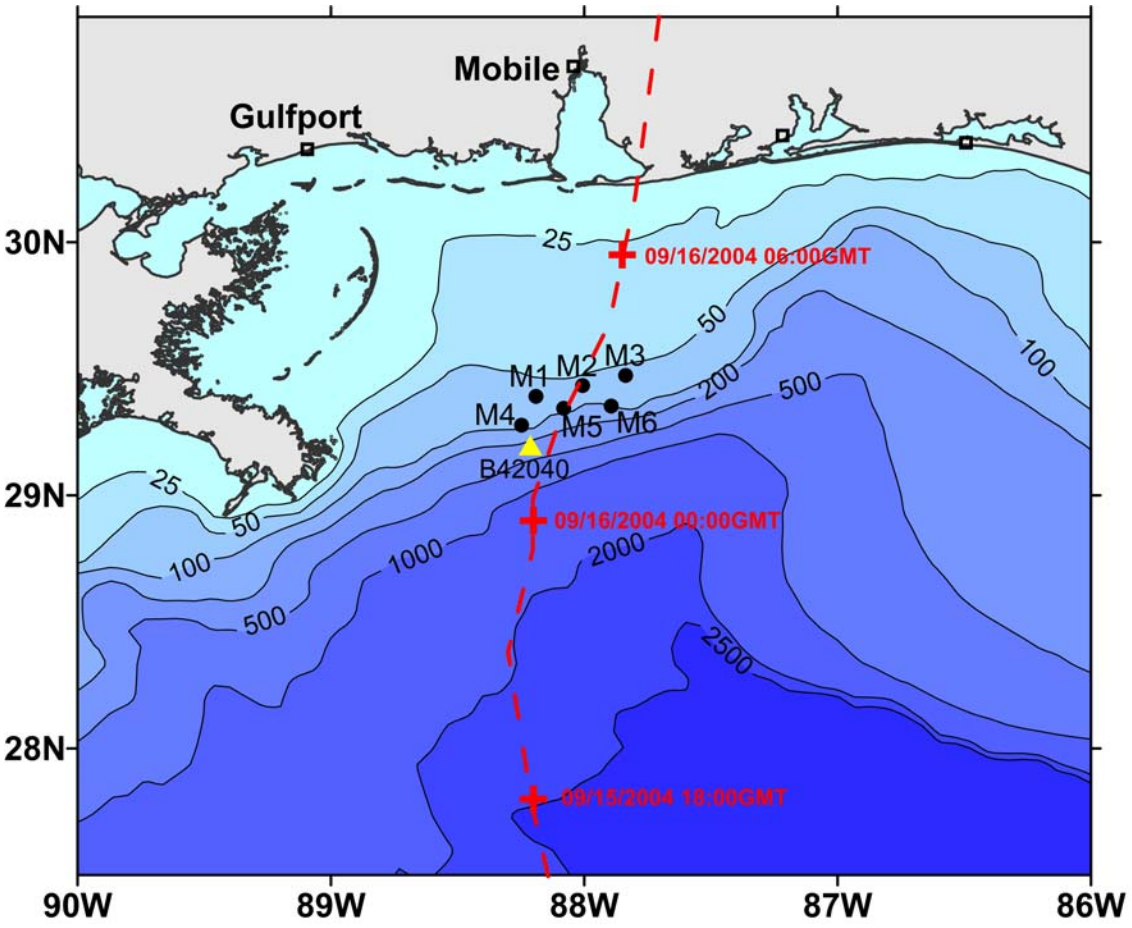
Mobile
Gulfport
30N
29N
28N
90W
89W
88W
87W
86W
25
50
100
200
500
1000
2000
2500
M1
M2
M3
M4
M5
M6
B42040
09/16/2004 06:00GMT
09/16/2004 00:00GMT
09/15/2004 18:00GMT

Figure 1

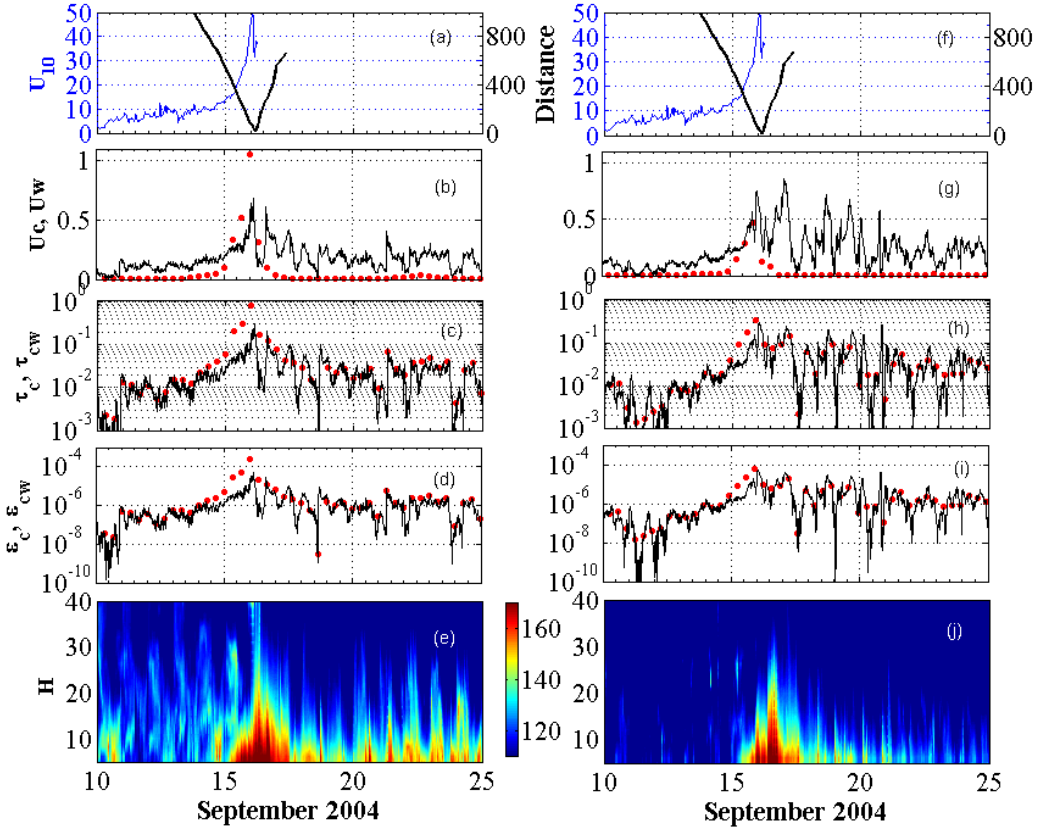
(a)
(b)
(c)
(d)
(e)
(f)
(g)
(h)
(i)
(j)
U10
Distance
Uc, Uw
τc, τcw
εc, εcw
H
September 2004
September 2004

Figure 2

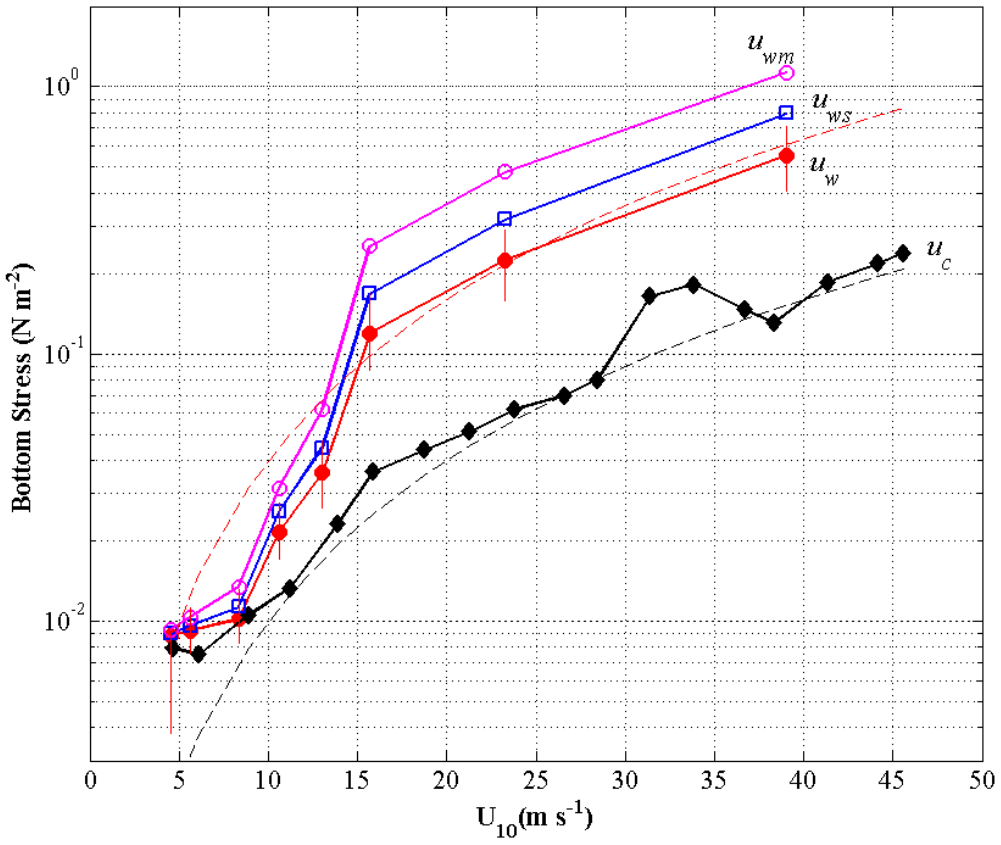

335
336
337 **Figure 3**